

Understanding the $L_{2,3}$ x-ray absorption spectra of early $3d$ transition elements

Robert Laskowski and Peter Blaha

Institute of Materials Chemistry, Vienna University of Technology, Getreidemarkt 9/165TC, A-1060 Vienna, Austria

(Received 1 September 2010; published 3 November 2010)

In this work we calculate the x-ray absorption spectra at the $L_{2,3}$ edges of the early $3d$ elements by solving the Bethe-Salpeter equation. We focus our discussion on the origin of the observed deviation of the branching ratio between L_2 and L_3 edges from its statistical value. Using the absorption edge of Ca in CaF_2 we show that the deviation is related to the mixing between the excitations from $2p_{1/2}$ and $2p_{3/2}$ core levels. Furthermore we find that the mixing is triggered by the exchange term of the electron-hole Hamiltonian. This term does not depend on the dielectric function, therefore such coupling is also present in metals explaining the high values of the branching ratios observed in the metals Ca and Ti. The calculated Ti $L_{2,3}$ spectra of SrTiO_3 and the anatase and rutile phases of TiO_2 reproduce even all fine details of the experimental spectra.

DOI: [10.1103/PhysRevB.82.205104](https://doi.org/10.1103/PhysRevB.82.205104)

PACS number(s): 73.20.At, 73.22.-f, 78.70.Dm

I. INTRODUCTION

X-ray absorption spectroscopy (XAS) measures the transitions between the core states of a particular atom and the conduction bands of the solid. It is one of the most important tools for the characterization of the unoccupied part of the electronic spectrum of materials.¹ Within the independent particle approximation (IPA) the XAS spectra are proportional to the unoccupied part of the projected density of states (DOS) weighted by the momentum matrix elements between the core and the conduction states. However, due to the localization of the core wave function the interaction of the excited electron with its hole (core hole) is very strong and cannot be neglected. In a first approximation such interactions can be included already within the IPA by using the final state rule and performing so-called “core-hole” calculations. In such calculations an electron is removed from a core level and added to the conduction band. In addition a supercell approach must be used and by constructing a large unit cell one ensures that the core holes do not interact with each other.^{2,3} Such core-hole calculations lead to fairly accurate results for K edges but it is also known that they fail reproducing the $L_{2,3}$ edges for early $3d$ elements. In particular, the so-called branching ratio between the L_2 and L_3 edges cannot be explained, within the IPA the branching ratio is always determined by the occupation numbers of the corresponding core states and in the case of $L_{2,3}$ edges this gives 1:2. However the observed ratios are much closer to 1:1 or even higher for K, Ca, Sc, Ti, and V.

In order to properly calculate such spectra an approach that goes beyond the IPA has to be used. One of the most accurate approaches is the *ab initio* configuration interaction method.^{4,5} However, the method cannot be applied to extended systems but the solid has to be approximated by a (very) small cluster. It has been applied successfully to various transition-metal oxides^{5,6} with localized ($3d$) conduction band states. A linear-response method based on time-dependent density-functional theory with a proper interaction kernel also leads to promising results. It has been applied mostly to metals.^{7,8}

Another approach that operates within many-body perturbation theory solves the Bethe-Salpeter equation (BSE).^{9–11}

In practice BSE is simplified to an eigenvalue equation,

$$\sum_{h'e'k'} H_{hek,h'e'k'}^e A_{h'e'k'}^\lambda = E^\lambda A_{hek}^\lambda. \quad (1)$$

The electron-hole Hamiltonian H^e consists of three terms,

$$H_{hek,h'e'k'}^{diag} = (\varepsilon_{hk} - \varepsilon_{ek} + \Delta) \delta_{hh'} \delta_{ee'} \delta_{kk'}, \quad (2)$$

$$H_{hek,h'e'k'}^{dir} = - \int d^3x d^3x' \psi_{hk}(\mathbf{x}) \psi_{ek}^*(\mathbf{x}') \times W(\mathbf{r}, \mathbf{r}') \psi_{h'k'}^*(\mathbf{x}) \psi_{e'k'}(\mathbf{x}'), \quad (3)$$

$$H_{hek,h'e'k'}^x = \int d^3x d^3x' \psi_{hk}(\mathbf{x}) \psi_{ek}^*(\mathbf{x}) \times \bar{v}(\mathbf{r}, \mathbf{r}') \psi_{h'k'}^*(\mathbf{x}') \psi_{e'k'}(\mathbf{x}'). \quad (4)$$

The H^{diag} term depends only on the energies of the occupied ε_{hk} (holes), and unoccupied ε_{ek} (electron) quasiparticle states, and accounts for a response in the noninteracting limit. The exchange H^x and the direct H^{dir} Coulomb terms couple the electron-hole pairs.¹² The exchange H^x term contains the short-range part of the bare Coulomb electron-hole interaction. $[\bar{v}(\mathbf{r}, \mathbf{r}')]$ The direct term, in principle, involves the dynamically screened Coulomb electron-hole interaction $[W(\mathbf{r}, \mathbf{r}', \omega)]$ and the excitation energies (E^λ), leading to a nonlinear eigenvalue problem. Therefore only static screening is taken into account, implying the assumption that the excitation energies E^λ are close to appropriate energy differences between conduction and valence bands. This approximation may be questioned when applied to the calculations of XAS, due to the rather large expected exciton binding energies. However, as we are going to show, it leads to a rather good agreement with measured spectra. The coupling coefficients (A^λ) define the electron-hole correlation function and enter the expression for the imaginary part of the dielectric function,

$$\varepsilon_2^{xy}(\omega) = \frac{8\pi^2}{\Omega} \sum_{\lambda} \left| \sum_{hek} A_{hek}^{\lambda} \frac{\langle h\mathbf{k} | -i\nabla_x | e\mathbf{k} \rangle}{\varepsilon_{e\mathbf{k}} - \varepsilon_{h\mathbf{k}}} \right|^2 \times \delta(E^{\lambda} - \omega). \quad (5)$$

The BSE approach is very successful in dealing with excitons and the response in the optical regime. It has also been applied previously to XAS, for K and L edges.^{13–18} It has been shown that for K edges of light elements it gives very similar results as standard DFT core-hole calculations.¹⁷

In this work we apply an all electron BSE formalism to calculate the $L_{2,3}$ absorption spectra of early $3d$ elements. We focus on fcc Ca, CaF_2 , SrTiO_3 , and TiO_2 in rutile and anatase structure and discuss, in particular, the deviation of the $L_{2,3}$ branching ratio from its statistical value. We also show that the method can be applied to calculate with a reasonable accuracy the L edges of heavier elements in the $3d$ row. The full-potential linearized augmented plane wave plus local orbitals method as implemented in the WIEN2K package¹⁹ has been used to compute the single-particle states.^{20,21} In our BSE implementation core and conduction states are calculated by solving separate eigenvalue problems. For nonmagnetic materials the core states are calculated by solving the radial Dirac equation using the spherical part of the total potential.²² This yields the numerically exact solutions (for a given potential) and the full spin-orbit splitting. In magnetic cases we use our regular spin-orbit coupling solver with scalar-relativistic basis functions²³ applied to a narrow eigenvalue window around the core states. Tests on nonmagnetic cases shows that this approach leads to an about 10% reduced spin-orbit splitting of the $2p$ shell because we lack $p_{1/2}$ -type basis functions and the standard scalar-relativistic p orbitals are only able to describe well the $p_{3/2}$ radial functions. In all calculations the conduction bands have been calculated using the scalar relativistic plus spin-orbit coupling method but the scalar-relativistic orbitals are good basis functions for both, $d_{3/2}$ and $d_{5/2}$ states and full spin-orbit splitting can be obtained. Our BSE solver is based on a plane-wave expansion of the dielectric function.¹² The matrix elements of the BSE Hamiltonian with localized core wave functions converge relatively slowly with respect to the plane-wave cutoff (g_{\max}). Therefore, depending on the case, we had to use large values of g_{\max} up to 12–15 a.u.⁻¹, while valence BSE requires usually g_{\max} of only 3–5 a.u.⁻¹ The theoretical spectra are broadened by a Lorentzian of 0.15 eV.

II. RESULTS

In Fig. 1 we have collected results of several different calculations of the Ca $L_{2,3}$ edge in CaF_2 illustrating the effect of various approximations to the electron-hole correlation. The experimental $L_{2,3}$ edge presented in Fig. 1(a) shows well isolated L_2 (higher energies) and L_3 branches with a ratio close to 1:1. Each branch contains two peaks, the first one is small, the second one large. The two peaks are separated by 1.6 eV and 1.3 eV in the L_3 and L_2 branches, respectively. The distance between the main L_2 and L_3 peaks is approximately equal to 3.2 eV. It is usually interpreted as pure spin-orbit splitting of the $2p$ core states but the DFT spin-orbit splitting of Ca $2p$ is significantly larger (3.69 eV). The

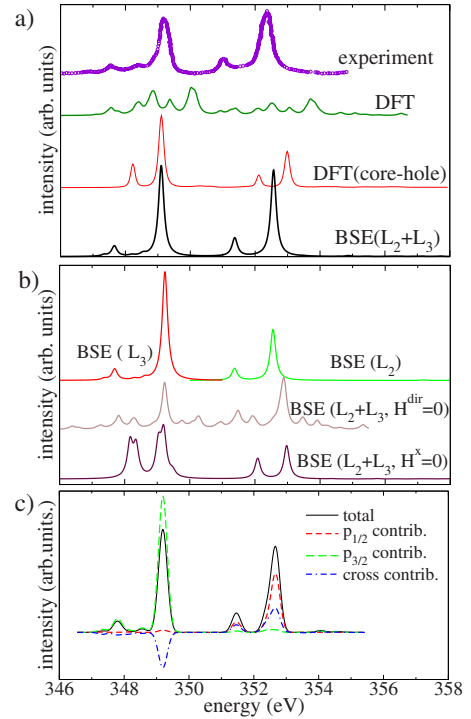


FIG. 1. (Color online) (a) Experimental CaF_2 L_2 (right) and L_3 (left) edges (Ref. 16) and calculations within ground-state DFT, using a supercell DFT core-hole approach and with the current BSE method. (b) BSE calculations when certain parts of the Hamiltonian are set to zero. For the line labeled as BSE (L_2) and BSE (L_3) the excitations from $2p_{3/2}$ and $2p_{1/2}$ core levels are not allowed to interact, for BSE ($L_{2,3}, H^{\text{dir}}=0$) the direct Coulomb term of the Hamiltonian is set to zero, and for BSE ($L_{2,3}, H^x=0$) the exchange part is neglected. (c) Decomposition of the spectrum into contributions involving squared matrix elements from $2p_{1/2}$ and $2p_{3/2}$ states as well as the coherent cross terms between these excitations.

ground-state DFT calculations [Fig. 1(a)] are not able to reproduce any feature of the experimental spectra because they neglect the electron-hole interaction completely. On the other hand in the supercell core-hole calculations the static Coulomb effect of the core hole is taken into account. In this case the shape of the calculated spectra shows a lot of similarities with the experimental curve and the spectral weight localizes into two peaks. Still important details are not reproduced: the separation of the small and the large peaks in each branch is too small, the separation of the branches is too large, and of course the branching ratio (L_2/L_3) has the statistical value equal to 1:2. It should be stressed that the results of the core-hole calculations are very sensitive to the size of the super cell. For converged results we had to use a primitive cubic $3 \times 3 \times 3$ cell with 324 atoms and 15 Å lattice parameter. Thus such calculations are fairly expensive and not “cheap” ground-state calculations anymore. The results of the BSE calculations with statically screened electron-hole interaction presented in Fig. 1(a) as curve BSE (L_2+L_3) show perfect agreement with experiment. In this case both, the separation of the main peaks and the branching ratio are close to the experimental values. Moreover, it appears that the main peaks in this spectra are dominated by single excitations indicating the strong excitonic character of these

peaks. We should mention here that for all calculated spectra the absolute transition energy edge has been adjusted according to the experimental edge. The calculated absolute transition energy edges are usually wrong by about 10%. This is related to the fact that the single-particle eigenvalues are not good approximation to the ionization energies and the errors are considerably different for core and conduction states. The situation can be partially improved by using the concept of Slater's transition state,²⁴ however this issue is out of the scope of the current work.

In order to interpret and analyze the success of the BSE calculations we present in Fig. 1(b) results of various calculations where some parts of the BSE Hamiltonian has been set to zero. The curves labeled as BSE (L_2) and BSE (L_3) result from BSE calculations where the excitations from the $2p_{1/2}$ and $2p_{3/2}$ states are not allowed to interact with each other. Here, the position of the peaks is the same as in the full BSE calculation [Fig. 1(a)] but the branching ratio is now equal 1:2. This clearly indicates that the nonstatistical branching ratio is a result of the coherent mixing between the excitations from the $2p_{1/2}$ and $2p_{3/2}$. It can be seen more directly in Fig. 1(c) where the decomposition of the spectrum into contributions from $p_{1/2}$ and $p_{3/2}$ states as well as their coherent cross term due to the squared matrix elements is shown. Clearly there is a negative cross-term contribution for the L_3 edge but an enhancement of the L_2 edge intensity. It should be stressed that the actual contributions from $p_{1/2}$ into the excitonic correlation functions of the L_3 edge and vice versa are rather small and do not exceed 2%. Shirley¹⁶ identified "multipole interactions" as responsible for the observed branching ratio of the Ti $L_{2,3}$ edge in SrTiO₃. Our findings at this point fully supports his conclusions but in our approach we go further and we demonstrate the individual effects of the direct and exchange terms of the BSE Hamiltonian [Eq. (2)] by performing calculations where one of these terms is set to zero [Fig. 1(b)]. Without the direct term the shape of the spectra becomes similar to the ground-state DFT result [Fig. 1(a)] but interestingly the branching ratio is still close to 1:1. On the other hand when the exchange term is set to zero the spectrum still resembles the results of the full calculations, but the branching ratio drops to 1:2, indicating that the exchange term is responsible for the high branching ratio. Since the exchange term does not depend on the screening, the mixing between the excitations from $2p_{1/2}$ and $2p_{3/2}$ levels should also be present for metals. Indeed, unusual branching ratios are also observed for the early $3d$ metals. The calculated spectrum for fcc Ca is presented in Fig. 2 and reproduces the experiment very well. This observation can be explained considering the spinor structure of the core states entering the expressions for the exchange and the direct terms of the BSE Hamiltonian. The spin part of the integral in the direct term separates the pairs of the conduction (ee') and the core (hh') states. Assuming the hydrogenic solution for the $2p_{1/2}$ and $2p_{3/2}$ core states, one can notice that the spin part of the integral in the direct term is zero. This leaves the exchange term as the only one coupling the L_2 and L_3 branches.

In order to see if the BSE approach is able to capture correctly the small differences resulting from different local atomic structures we have calculated the $L_{2,3}$ edges of Ti in

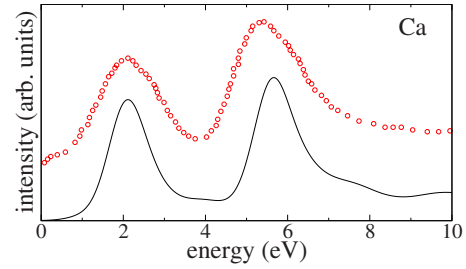


FIG. 2. (Color online) The calculated (solid line) and experimental $L_{2,3}$ edges of fcc Ca (experiment taken from Ref. 25).

SrTiO₃ and the rutile and anatase modifications of TiO₂. SrTiO₃ is cubic and Ti is surrounded by a perfect oxygen octahedron while the tetragonal TiO₂ modifications have differently distorted octahedra. The results of our calculations together with the experimental data are presented in Fig. 3. For all three compounds the L_2 and L_3 edges are well separated by about 5.65 eV. The branching ratio is approximately 1:1 and within each edge the peaks are separated by about 2.4 eV. The differences between the three materials concern mainly the shape of the second peak in the L_3 spectra. SrTiO₃ exhibits a rather symmetric and regular peak, while anatase has a well visible shoulder at the right side (higher energy), whereas for rutile the shoulder appears at the left

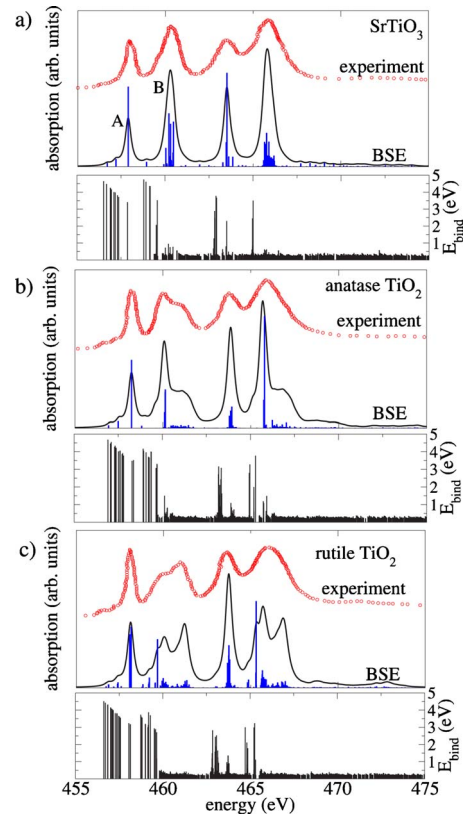


FIG. 3. (Color online) Calculated (full line) and experimental (dotted curve, taken from Ref. 26) Ti $L_{2,3}$ edges in (a) SrTiO₃, (b) TiO₂ anatase, and (c) TiO₂ rutile within the BSE formalism. In the upper panels we show also bars indicating the oscillator strength of the excitons while in the lower panels the corresponding binding energies are displayed.

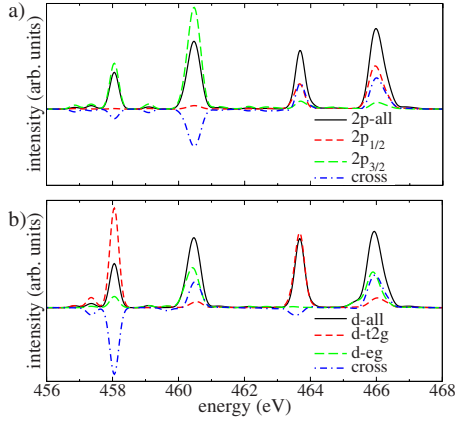


FIG. 4. (Color online) Decomposition of the $L_{2,3}$ edge of SrTiO₃ calculated within BSE into contributions involving (a) excitations from $2p_{1/2}$ and $2p_{3/2}$ states (b) excitations into $d-e_g$ and $d-t_{2g}$ states as well as their coherent cross terms.

side. The calculated spectra reproduce these subtle features very good. This is in contrast to the results presented by Shirley¹⁶ where particularly for rutile TiO₂ the ratio of the peaks in the branches is wrong. However our results agree very well with the multichannel multiple-scattering calculations of Krüger.¹⁸ In the lower panels we show the binding energies of the excitations, defined as the average difference between the quasiparticle energies and the excitation energy $E_{bind}^\lambda = \sum_{k,e,h} A_{k,h,e}^2 (\epsilon_{ek} - \epsilon_{hk} - E_\lambda)$. A large binding energy of a particular excitation usually indicates a strong excitonic character but we can see that most excitons have vanishing oscillator strength and do not contribute to the spectrum (bars in the upper panels of Fig. 3). For SrTiO₃, however, the first L_3 peak corresponds to a single excitation with a large binding energy and this results in the separation of this peak from the second one, which originates from several excitations with rather small binding energies. A similar analysis holds for the L_2 spectrum and for rutile and anatase TiO₂. However, in the TiO₂ cases the second L_3 peak also contains some excitations with higher binding energy and this results in a splitting of this peak and the generation of the observed shoulders. The branching ratio is again determined by the cross terms between $2p_{1/2}$ and $2p_{3/2}$ core states. Figure 4(a) shows the decomposed dielectric function of SrTiO₃ with respect to the core states. Similar as in CaF₂ the L_3 and L_2 edges contain small components from the $2p_{1/2}$ and $2p_{3/2}$ states, respectively, and via destructive and constructive cross terms the branching ratio is modified significantly.

The splitting of the L_2 or L_3 edge into doublets is often understood as a result of the crystal-field splitting of the $3d$ states into t_{2g} and e_g .²⁶ However, our results indicate that such an interpretation is too simple, which is also evident from the fact that the ratio of the intensities of the two peaks is not 3:2 as expected from the number of d electrons in the corresponding bands. Figure 4(b) shows the contributions of the $d-e_g$ and $d-t_{2g}$ conduction bands to the dielectric function of SrTiO₃. As expected, the first peak of each branch originates mainly from excitations into $d-t_{2g}$ states, while $d-e_g$ dominates the second one, but the oscillator strength of all peaks is strongly modified by cross terms between $d-t_{2g}$ and

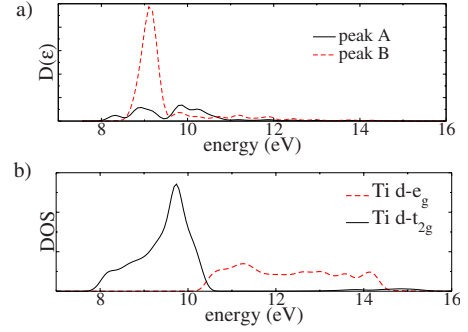


FIG. 5. (Color online) (a) Decomposition of the conduction-band components of the BSE eigenstates contributing to the calculated L_3 edge of SrTiO₃. The quantity $D(\epsilon)$ is defined as: $D(\epsilon) = \sum_i \sum_{k,h,e} A_{k,h,e}^2 \times f_i \times \delta(\epsilon - \epsilon_{ek})$, where f_i is the oscillator strength and the sum runs over the states contributing to the A and B peaks of the L_3 edge, respectively. $D(\epsilon)$ is essentially the density of states of the conduction bands extracted from these peaks. (b) The ground-state Ti $3d-e_g$ and Ti $3d-t_{2g}$ DOS of SrTiO₃.

$d-e_g$ in the squared momentum matrix elements [see Eq. (5)]. This can reduce (first L_3 peak) or enhance (second L_3 and L_2 peak) the intensities by a factor of 2. Surprisingly, when we examine the decomposition of the electron-hole states [given by $D(\epsilon)$ in Fig. 5(a)] of the two peaks A and B of the L_3 edge, we notice that most of the weights originate from conduction bands that are of Ti $3d-t_{2g}$ character. Peak A stems from only three very localized excitons with a large binding energy E_{bind}^λ and large oscillator strength. It has contributions from a wide range of conduction bands including both, t_{2g} and e_g states, however, as was shown in Fig. 4(b), the t_{2g} contributions to the dielectric function dominates due to matrix element effects. On the other hand, peak B originates from several $e-h$ states with smaller binding energy and their $D(\epsilon)$ [Fig. 5(a)] is strongly peaked in the $3d-t_{2g}$ region. Nevertheless matrix element effects drastically reduce the t_{2g} contribution to the total intensity of peak B and $3d-e_g$ contributions dominate the optical response. Considering this analysis, the splitting of the L_3 edge into two peaks A and B is related to a large extent to the differences in the binding energies of the excitons and not so much to the t_{2g}/e_g splitting of the conduction bands. This explains then why the energy separation between the two peaks cannot be represented well by core-hole DFT calculations (Fig. 1). We conclude this part of the discussion with a warning that one has to be careful when interpreting the decomposition of a BSE eigenstate, which could be a linear combination of many conduction band states, but only some of them are optically active.

We can see from the above discussion that the BSE rather well reproduces the experimental $L_{2,3}$ edges of $3d^0$ ions such as Ca²⁺ and Ti⁴⁺. In the case of elements with a nonempty $3d$ shell the interaction between the excited electron and the electrons already present in the shell complicates the situation. However as we can see in Fig. 6 where the results for MnO [Fig. 6(a)] and CoO [Fig. 6(b)] are presented the overall quality of the calculated spectra is rather good, the main features of the measured $L_{2,3}$ edges are reproduced. The underestimated value of the spin-orbit splitting between L_2 and

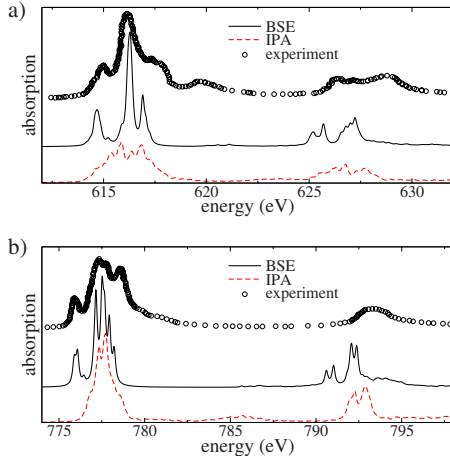


FIG. 6. (Color online) $L_{2,3}$ edges calculated for (a) MnO and (b) CoO. The single-particle states has been calculated using on-site hybrid exchange energy functionals (Ref. 27).

L_3 branches is related to the approximate method used for calculating the core states, as it was explained in Sec. I. Moreover, it is obvious that the agreement with experiment would improve if we were able to improve the description of electron-electron interaction in the $3d$ shell. For example, in the *ab initio* configuration interaction method^{4,5} this interaction is fully included, and in the case when the excitons are localized within the metal- O_6 cluster this method gives excellent agreement with experiment.

The origin of the nonstatistical branching ratio is related to the coupling between excitation from $2p_{1/2}$ and $2p_{3/2}$ core states. Such a coupling depends sensitively on the magnitude of the spin-orbit splitting between these states. In order to demonstrate this we have recalculated the spectra of rutile TiO_2 where the separation between the Ti $2p_{1/2}$ and Ti $2p_{3/2}$ levels has been gradually increased from 5.65 to 25 eV. The resulting branching ratios are plotted as a function of the spin-orbit splitting in Fig. 7 and are compared to the directly calculated branching ratios as well as the estimated ratios from the experimental curves for other $3d$ systems. As we can see the values drop quite fast when the splitting increases, approaching asymptotically the statistical value. It reproduces the overall trend of the experimental points indicating that the size of the spin-orbit splitting is in fact the most important factor that determines the strength of the coupling.

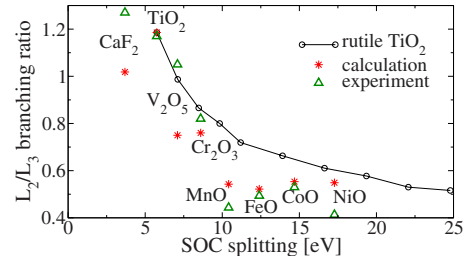


FIG. 7. (Color online) The dependence of the $L_{2,3}$ branching ratio in rutile TiO_2 as a function of the spin-orbit splitting of the $2p_{1/2}$ and $2p_{3/2}$ states compared to experimental and calculated ratios of the various $3d$ metals.

III. CONCLUSIONS

In this paper we have demonstrated that an all-electron fully relativistic BSE method with standard static screening of the electron-hole interaction can be used to calculate the $L_{2,3}$ edges of $3d$ transition metals, leading to good agreement with the measured spectra. Most importantly we have identified that the nonstatistical branching ratio is the results of the coherent mixing between the excitations from the $2p_{1/2}$ and $2p_{3/2}$ core states. The coupling of these terms occurs due to the exchange part of the BSE Hamiltonian. It is also present in metals as shown for fcc Ca. These effects are indirectly proportional to the size of the spin-orbit splitting and thus for later transition metals they become smaller until finally the statistical branching ratio of 1:2 is reached. Similar mechanism affects the ratio between the $d-t_{2g}$ and $d-e_g$ peaks in the Ti edges. We have demonstrated that the commonly assumed interpretation of the two prominent peaks of an L_3 or L_2 spectrum as pure crystal-field splitting ($d-t_{2g}$ and $d-e_g$) is oversimplified and important cross terms between these bands modify the observed intensities significantly. The direct screened Coulomb interaction is responsible for the localization of the spectrum into a few characteristic peaks and this is of course completely missing in ground-state DFT calculations. The BSE method is even able to capture the fine details and differences in the Ti $L_{2,3}$ edges of $SrTiO_3$ and rutile or anatase TiO_2 . We identified the left and right shoulders of the second L_3 peak in rutile and anatase due to excitations with large and small exciton binding energies, respectively.

ACKNOWLEDGMENT

We acknowledge support from the Austrian Science Fund FWF for project SFB-F41 (ViCoM).

¹J. J. Rehr and R. C. Albers, *Rev. Mod. Phys.* **72**, 621 (2000).

²V. Mauchamp, M. Jaouen, and P. Schattschneider, *Phys. Rev. B* **79**, 235106 (2009).

³I. Tanaka and T. Mizoguchi, *J. Phys.: Condens. Matter* **21**, 104201 (2009).

⁴Y. Kumagai, H. Ikeno, and I. Tanaka, *J. Phys.: Condens. Matter* **21**, 104209 (2009).

⁵H. Ikeno and I. Tanaka, *Phys. Rev. B* **77**, 075127 (2008).

⁶H. Ikeno, F. M. F. de Groot, E. Stavitski, and I. Tanaka, *J. Phys.:*

Condens. Matter **21**, 104208 (2009).

⁷J. Schwitalla and H. Ebert, *Phys. Rev. Lett.* **80**, 4586 (1998).

⁸A. L. Ankudinov, A. I. Nesvizhskii, and J. J. Rehr, *Phys. Rev. B* **67**, 115120 (2003).

⁹G. Strinati, *Phys. Rev. Lett.* **49**, 1519 (1982).

¹⁰S. Albrecht, L. Reining, R. Del Sole, and G. Onida, *Phys. Rev. Lett.* **80**, 4510 (1998).

¹¹M. Rohlfing and S. G. Louie, *Phys. Rev. Lett.* **81**, 2312 (1998).

¹²M. Rohlfing and S. G. Louie, *Phys. Rev. B* **62**, 4927 (2000).

- ¹³E. L. Shirley, *Phys. Rev. Lett.* **80**, 794 (1998).
- ¹⁴J. A. Soininen and E. L. Shirley, *Phys. Rev. B* **64**, 165112 (2001).
- ¹⁵E. L. Shirley, *J. Electron Spectrosc. Relat. Phenom.* **136**, 77 (2004).
- ¹⁶E. L. Shirley, *J. Electron Spectrosc. Relat. Phenom.* **144-147**, 1187 (2005).
- ¹⁷W. Olovsson, I. Tanaka, T. Mizoguchi, P. Puschnig, and C. Ambrosch-Draxl, *Phys. Rev. B* **79**, 041102 (2009).
- ¹⁸P. Krüger, *Phys. Rev. B* **81**, 125121 (2010).
- ¹⁹P. Blaha, K. Schwarz, G. K. H. Madsen, D. Kvasnicka, and J. Luitz, *WIEN2k: An Augmented Plane Wave Plus Local Orbitals Program for Calculating Crystal Properties* (Vienna University of Technology, Austria, 2001).
- ²⁰P. Puschnig and C. Ambrosch-Draxl, *Phys. Rev. B* **66**, 165105 (2002).
- ²¹R. Laskowski and N. E. Christensen, *Phys. Rev. B* **74**, 075203 (2006).
- ²²J. P. Desclaux, *Comput. Phys. Commun.* **1**, 216 (1970).
- ²³A. H. MacDonald, W. E. Pickett, and D. D. Koelling, *J. Phys. C* **13**, 2675 (1980).
- ²⁴K. Schwarz, *Chem. Phys.* **7**, 100 (1975).
- ²⁵J. Fink, T. Müller-Heinzerling, B. Scheerer, W. Speier, F. U. Hillebrecht, J. C. Fuggle, J. Zaanen, and G. A. Sawatzky, *Phys. Rev. B* **32**, 4899 (1985).
- ²⁶G. van der Laan, *Phys. Rev. B* **41**, 12366 (1990).
- ²⁷F. Tran, P. Blaha, K. Schwarz, and P. Novák, *Phys. Rev. B* **74**, 155108 (2006).